Graphene Oxide as a Monoatomic Blocking Layer

Søren Petersen,[†,#] Magni Glyvradal,[‡,#] Peter Bøggild,[§] Wenping Hu,[⊥] Robert Feidenhans'l,[‡] and Bo W. Laursen[†,*]

[†]Nano-Science Center & Department of Chemistry, University of Copenhagen, Copenhagen, Denmark, [‡]Nano-Science Center & Niels Bohr Institute, University of Copenhagen, Copenhagen, Denmark, [§]DTU Nanotech, Technical University of Denmark, Lyngby, Denmark, and [⊥]Institute of Chemistry, Chinese Academy of Sciences, Beijing, China. [#] These authors contributed equally.

ABSTRACT Monolayer graphene oxide (mGO) is shown to effectively protect molecular thin films from reorganization and function as an atomically thin barrier for vapor-deposited Ti/Al metal top electrodes. Fragile organic Langmuir–Blodgett (LB) films of C_{22} fatty acid cadmium salts (cadmium(II) behenate) were covered by a compressed mosaic LB film of mGO flakes. These hybrid LB films were examined with atomic force microscopy (AFM) and X-ray reflectivity, both with and without the metal top electrodes. While the AFM enabled surface and morphology analysis, the X-ray reflectivity allowed for a detailed structural depth profiling of the organic film and mGO layer below the metal top layers. The structure of the mGO-protected LB films was found to be perfectly preserved; in contrast, it has previously been shown that metal deposition completely destroys the first two LB layers of unprotected films. This study provides clear evidence of the efficient protection offered by a single atomic layer of GO.

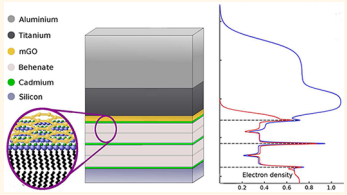

KEYWORDS: graphene oxide · molecular electronics · vertical devices · barrier layer · molecular interfacing · X-ray reflectivity

The concept of molecular electronics has been demonstrated in devices such as memory switches, transistors, and rectifiers[1−3] and is now emerging as a key technology due to the need for miniaturization and advanced functions of electronic devices.[4,5] Recent progress shows great promise for practical uses of molecular electronics.[6,7] One of the important elements in fabricating such devices is the control over the interfaces between the different components on a close to atomic scale. Making well-defined atomically abrupt interfaces between metal connects and an organic device has however proven to be a major challenge. One consequence is that unambiguous characterization of the systems is severely hampered by this limitation of the test beds.[8,9] One of the most common approaches is to place molecules in a metal−molecule−metal junction, such as single-molecule junctions formed by self-assembly in break junctions[3,5,10−12] or with an ensemble layer of molecules in parallel connection between macroscopic electrodes in vertical devices, *e.g.*, the crossbar junction.[13−16] Of these, the crossbar junction approach seems most scalable for complex, permanent devices and ultimately for technological applications. The primary method for depositing the second (top) electrode is vapor deposition of metals. Compared to many molecular electronics concepts, this approach has the great advantage of easy patterning of complex circuitries and has the potential for upscaling. However, it suffers from substantial short circuits and filamentary growth through the thin films of both chemisorbed and physisorbed molecular layers.[17−19] Several strategies have been developed in order to circumvent this penetration problem by changing the electrode deposition method, geometry, and material, *e.g.*, nanotransfer printing,[20,21] nanopores,[22] crossed wires,[23] mercury drops,[24] and use of conductive organic interlayer materials such as poly(3,4-ethylenedioxythiophene)-stabilized with poly(4-styrenesulfonic acid) (PEDOT:PSS).[6] None of these approaches are able to make atomically thin protecting layers, nor have they provided a general applicable solution to the problem.

Since the seminal work in 2004−2005, graphene has received an unprecedented amount of attention due to its unique electronic properties.[25−27] Furthermore, its two-dimensional hexagonal carbon lattice[25,28] makes it impermeable to atomic diffusion.[29] As graphene is also extremely mechanically flexible, has a mechanical breaking strength of 42 N/m,[30] and absorbs only 2.3% of the visible light per layer,[31] it is in particular suitable for transparent electrodes in flexible electronics and photovoltaics.[32−35] Recently, thin films of chemical vapor deposited (CVD) graphene and spin-cast reduced graphene oxide (RGO) were used as blocking layers

* Address correspondence to bwl@nano.ku.dk.

Received for review June 14, 2012 and accepted August 14, 2012.

Published online August 15, 2012
10.1021/nn302628q

© 2012 American Chemical Society

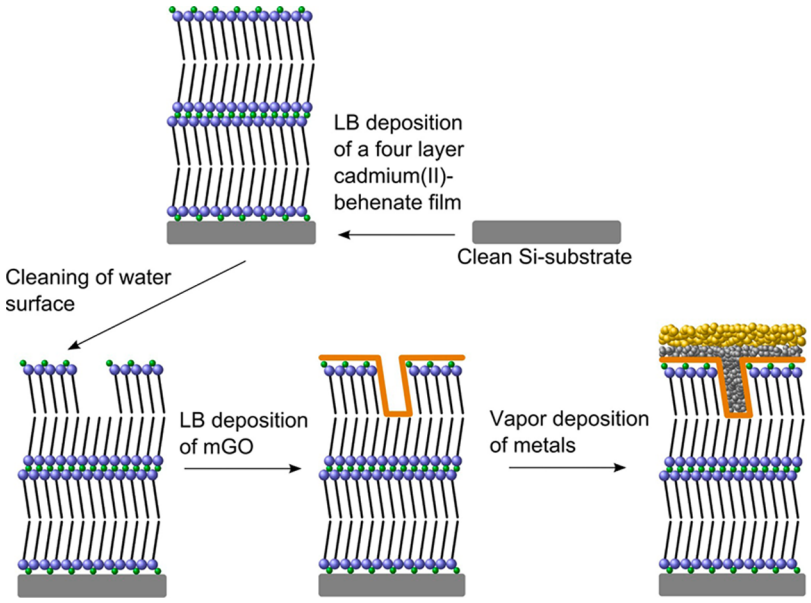

Figure 1. Deposition scheme of fatty acid-metal salt−mGO hybrid film. Four-layer Y-type LB films of cadmium(II) behenate were first deposited on cleaned Si wafers. Second, while the four-layer film was kept submerged, the water surface was thoroughly cleaned for lipids followed by deposition, compression, and vertical LB transfer of mGO flakes. Lastly, the LB hybrid film was covered by metal thin films. As illustrated, naturally occurring holes are formed in the fatty acid−metal salt film. Due to mGO's flexible nature, these atomically thin sheets follow the surface morphology perfectly. The holes are therefore filled partly by mGO and partly by Ti.

towards metal penetration in vertical devices.[36−38] The films consisted of multilayers with a thicknesses of about 10 nm, whereas the standard material (PEDOT:PSS) typically had a layer thickness of 90 nm.[6] Use of graphene materials is a major breakthrough for solving the top-contact problem of vertical molecular (crossbar) devices. Yet, these demonstrations still have a significant flaw; that is, the thickness is still 1 order of magnitude larger than the active layer. As demonstrated by Li *et al.*,[38] the vertical transport through the RGO thin film electrodes is not metallic nor is it described by tunneling, but is instead described by a thermally activated hopping mechanism, and when cooled, the resistance of the film increases to roughly one-tenth of an alkane monolayer. The hopping-type transport in the RGO multilayers poses a potential problem for analyzing and mapping electronic fingerprints of more interesting molecules with lower resistances. One solution to this problem is to reduce the interlayer thickness to an extent where tunneling through the interlayer becomes the dominant transport mechanism, which is expected to happen below 4 nm.[39,40]

Here we demonstrate that we can prepare and transfer a densely packed mosaic film of monolayer graphene oxide (mGO) flakes onto organic thin films using the LB deposition techniques and that this *mono*atomic GO layer functions as an efficient blocking layer toward metal penetration and reorganization at the interface. When using solution-processable mGO for vertical devices, no post-treatments are necessary such as annealing or acetone washing since in-plane conductivity should not matter, when the mGO will function only as an atomically thin tunnel barrier. The mGO mosaic LB films have the advantage of very gentle transfer to all types of hydrophilic thin films compatible with submersion in water and that high coverage of large areas (wafer scale) is generally straightforward.

RESULTS AND DISUSSION

To investigate the effectiveness of the mGO barrier layer, a particularly sensitive model system was chosen, *i.e.*, physisorbed LB thin films of a fatty acid−metal salt.[41] In a previous report,[19] we showed by using X-ray reflectivity that the two first layers of a five-layered lead(II) arachidate LB film were completely destroyed by vapor deposition of a titanium/aluminum top electrode. X-ray reflectivity is an ideal nondestructive technique for investigating interfacial reactions on the atomic scale.[42]

Besides their structural fragility, the LB films of a fatty acid−metal salt provide high contrast in the X-ray reflectivity depth profiling, where the heavy metal ions act as clear depth markers.[19] Unfortunately, the five-layer lead(II) arachidate LB films proved to be unsuitable for the present study, since these films were found to reorganize when rewetted during LB deposition of the mGO top layer (see Supporting Information for details). Instead, the hybrid LB films of cadmium(II) behenate and mGO were prepared in a one-pot preparation procedure, outlined in Figure 1; a four-layer LB film of cadmium(II) behenate is prepared, and while still in the subphase, the fatty acids were sucked off

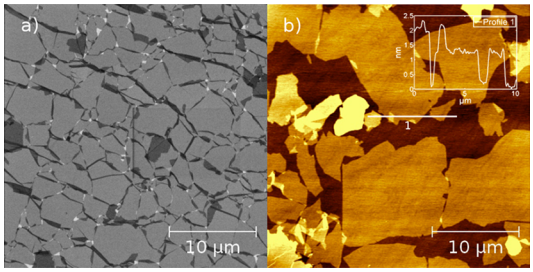

Figure 2. (a) SEM images of an overlapping mGO LB film on SiO_2. (b) AFM image of a loosely packed mGO LB film on SiO_2, confirming that the majority of the sheets seen in the SEM are indeed monolayers.

followed by deposition of an mGO LB film.[41,43,44] In this procedure the cadmium(II) behanate LB films were found to be sufficiently stable in the subphase to allow formation of the mGO Langmuir film and its subsequent transfer to the four-layer fatty acid LB film.[41]

The LB deposition of mGO is advantageous over spin-casting in several ways. It allows for deposition on fragile physisorbed films, such as the fatty acid−metal salts, and it enables excellent control over morphology and density of the mGO film.[43,45] This is very important for the present application, where holes in the mGO mosaic film would compromise its ability to protect the molecular film. In a neutral subphase with no predeposition of fatty acid−metal salt films and by control of the barrier pressure of the LB trough we were able to prepare dense, slightly overlapping mGO mosaic films (Figure 2a) consisting of 80 area % monolayer GO, 13 area % double layers (mainly overlapping edge regions), 6 area % multilayers, and only 1 area % uncovered (holes). The area analysis is based on the clear contrast difference in the SEM picture (Figure 2a), while AFM was used to confirm the assignment of mono- and double-layer regions (Figure 2b). The height profile confirms a layer thickness of ~1 nm, which according to literature agrees well with a monolayer GO sheet on SiO_2 at ambient conditions with a monolayer of water (0.37 nm) between the SiO_2 surface and the GO sheet.[43,46,47] The size of the mGO flakes is typically in the range of a few to hundreds of μm^2, with some sheets greater than 1000 μm^2.

In the hybrid LB films of cadmium(II) behenate and mGO the morphology of the mGO LB films was strongly dependent on which surface pressure the films were transferred at. In the hybrid films the mGO LB films were thus transferred at a surface pressure of 15 mN/m compared to 25−30 mN/m for the pure mGO LB film. Unless stated otherwise, the mGO LB films in the hybrid films were transferred at 15 mN/m. Characterization of hybrid films with mGO LB films transferred at higher surface pressures can be found in the Supporting Information. Two of the four samples created in each preparation were covered with 50 Å titanium and 100 Å aluminum by vapor deposition. The remaining two served as reference samples. The hybrid films were investigated with AFM and X-ray reflectivity. In Figure 3a, an AFM image is shown for a four-layer cadmium(II) behenate film with mGO, with its corresponding phase image (b), and with metals (c and d).

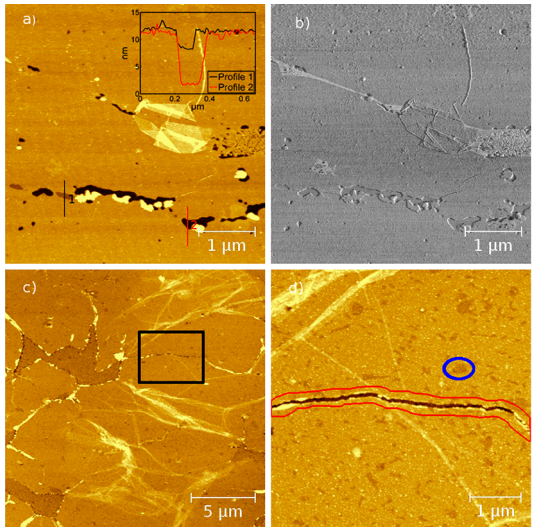

Figure 3. (a) AFM topography image of a four-layer cadmium(II) behenate film covered with an mGO mosaic film. Profiles 1 and 2 show a height difference of 3 and 9 nm, respectively, corresponding to monolayer and triple-layer holes. The height scale is 20 nm. (b) Corresponding phase image, showing a clear difference between covered and uncovered areas of the fatty acid film (light gray). As seen, a small uncovered band propagates through the upper left corner, which is not easily observed in the height image in (a). (c) Large-scale AFM topography image of a four-layer cadmium(II) behenate film covered with an mGO film and 50 Å Ti + 100 Å Al. Wrinkles formed by compression are clearly visible. (d) A close-up of the black square in (c) clearly showing the preservation of the morphology of the underlying fatty acid−metal salt film and the two types of holes. The 3 nm (monolayer) holes are seen as small dark brown regions (see blue circle), with areas ranging from a few to hundreds of square nanometers. The 9 nm (three-layer) holes are seen as black elongated regions, which are typically several micrometers long, highlighted with a red border. An increase in the surface roughness due to the metals is clearly visible as small dots. The height scale in both images (c) and (d) is 30 nm.

From the AFM images in Figure 3a and b several important features of the mGO-covered LB films can be extracted: (1) The dominating mGO-covered areas are ultraflat with an average roughness of less than 5 Å (without metal). (2) The mGO flakes follow the underlying surface morphology smoothly. This is clearly indicated by the presence of 3 and 9 nm depressions in the mGO flakes, where natural defects in the fatty acid LB film below are present, as seen from the two trace profiles inset in Figure 3a.[19,41,45,48,49] These defects correspond to the absence of one and three monolayers of the fatty acid cadmium salt, respectively, and are in prefect agreement with the reported height of a cadmium(II) behenate LB monolayer (30 Å).[50] In total these defects account for ~10% of the total surface area with large variations in density within the film. However, most of these defects (9−10 area %) are 3 nm deep defects, and very few (<1 area %) are 9 nm deep defects

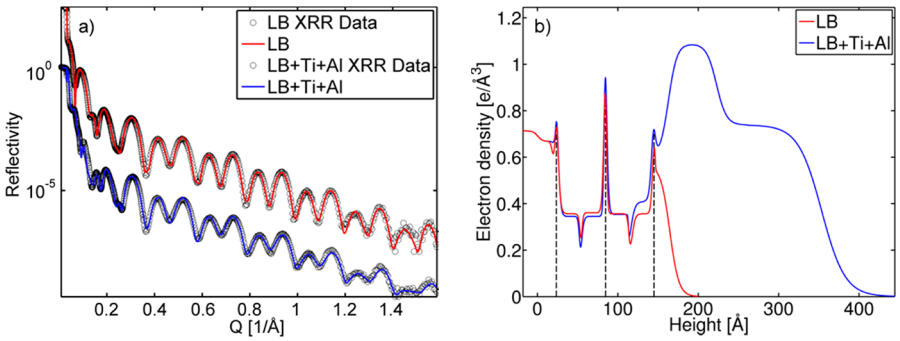

Figure 4. (a) X-ray reflectivity data for a four-layer cadmium(II) behenate + GO LB film on Si/SiO_2 (red) and a four-layer cadmium(II) behenate + GO LB film with 50 Å Ti + 100 Å Al on Si/SiO_2 (blue). The circles represent the data, while the solid lines correspond to the modeled fits. The red curve and the corresponding data set have been offset for clarity. (b) Corresponding electron density distributions calculated for the LB data (red curve) and the LB + Ti + Al data (blue curve). The dashed lines mark the position of the cadmium peaks.

(see Supporting Information for details). (3) Small areas of uncovered fatty acid LB film can be found between the edges of two mGO flakes and are most clearly seen in the AFM phase image as light gray regions and in the metal-covered films. The uncovered areas have a higher density of holes, as also discussed in the Supporting Information. On the basis of the contrast difference in the phase images, we analyzed the mGO coverage. We found that the surface coverage and morphology change slightly when depositing mGO on the fatty acid−metal salt films with Cd^{2+} ions in the subphase compared to depositing on planar SiO_2 with milli-Q water in the subphase. The coverage of monolayers decreases from 80 to 67 area %, double-layer coverage remains unchanged around 13 area % (now due to folding and not overlapping), multilayer coverage increases from 3 to ca. 10 area % (from wrinkles in mGO sheets), and uncovered area coverage increases from 1 to 10 area % (see Supporting Information for details). We propose that this increase in occurrence of folding and wrinkles is an effect of Cd^{2+} ions in the subphase that may coordinate to COO^- groups at the mGO edges and function as glue between the sheets.[51−53] Overlapping of sheets and closing of holes are then suppressed, and folding becomes the dominant mode of strain release. A similar effect was observed by Cote *et al.* for LB films of GO when changing the pH in the subphase from basic to acidic, resulting in hydrogen bonding between −COOH groups.[54] Despite this increase in wrinkles, we find that the surface roughness of these hybrid films is extremely low.

It was not possible to produce reference samples of four-layer cadmium(II) behenate without mGO, since the four-layer films without mGO were found to reorganize immediately after the films were pulled through the clean water surface (see Supporting Information for details). This finding further emphasizes the fragile nature of the unprotected fatty acid LB films.

After vapor deposition of 150 Å metal (50 Å Ti + 100 Å Al) additional important features can be extracted from the AFM images in Figure 3c and d: (1) An increase in the surface roughness (from 0.5 to 1 nm) is observed as the metals form small clusters on the surface. (2) The morphology of the underlying hybrid film is still clearly visible, giving a first indication of the protective effect of the mGO layer.

The detailed structure of the metal-covered composite films was mapped out using synchrotron X-ray reflectivity at the BW2 beamline at HASYLAB at DESY in Hamburg. In brief, in an X-ray reflectivity experiment, the reflected intensities from a sharp interface are measured as a function of the angle of incidence θ or, more commonly, as a function of the momentum transfer given by $Q = 2k \sin(\theta)$, where k is the wavevector of the photon. Below a critical angle for total reflection all X-ray photons are reflected, while at angles above the critical angle, the detailed intensity profile can be related back to the electron density profile along the surface normal by using simple inverse methods, as the scattering is kinematical. For multilayer films interference patterns act as fingerprints of the thin film structure.

The reflected X-ray intensity *versus* momentum transfer Q is shown in Figure 4a. The oscillations in the X-ray reflectivity arise from interference of scattering between the different layers in the film. The oscillations from the four-layer film with mGO are clearly preserved in the four-layer film with mGO and metals. The effect of the metal film on the X-ray reflectivity data is seen only at very small momentum transfers ($Q <$ 0.1 $Å^{-1}$), where the two reflectivity curves differ most. The rapid oscillations seen here arise from the thick metal film, and their fast decay indicates that the top surface of the metal film is fairly rough. The very small differences between the two curves at large Q are a strong indication that the structure of the organic film is preserved underneath the metal film with basically no change in the interfacial roughness, proving the effect of the monoatomic mGO as a blocking layer against metal penetration. In the derived electron density profiles (Figure 4b) the three signal peaks from Cd^{2+} ions at 23, 83, and 143 Å (dashed lines) above the Si/SiO_2

interface are clearly visible in both the film with and without metals, showing that even the structure of the topmost parts of the fatty acid−metal salt LB film is practically unaffected by the metal deposition. The electron density of the three peaks is as expected, with the first and the third peak containing half the number of electrons as the second peak (46 electrons from the Cd^{2+} and 20 electrons from 2 water molecules) due to coordination of cadmium with fatty acids from only one side giving half the amount of cadmium ions in the first and third peak (see Supporting Information for further details). It is noted that the vertical distance between the cadmium peaks is exactly 60 Å, in perfect agreement with the expected monolayer thickness of 30 Å. The slight dips in electron density after the first and third fatty acid layer observed at 30 and 90 Å from the first Cd^{2+} peak (Figure 4b) correspond to the interface between the two tails of the aliphatic carbon chains. The electron density δ of the behenate layers is as expected, around δ = 0.35−0.36 e/Å^3, for the first three layers. In the topmost monolayer of a fatty acid−metal salt an increase in electron density of ∼14% is observed, after metal deposition (Figure 4b). This can be explained by the presence of ∼10 area % natural holes in the LB film structure as discussed above, which will be filled with mGO and titanium. Assuming 10% of the top layer is filled with mGO and titanium, an increased electron density δ in the top layer is to be expected. The electron density is calculated to increase from δ = 0.36 e/Å^3 for the perfect lipid film with no holes to δ = 0.45 e/Å^3 for a film with 10% of the fatty acid layer replaced by holes filled with mGO and/or titanium (bulk value, 1.24 e/Å^3); see Supporting Information for detailed analysis and calculations. The values of the metals (titanium and aluminum) do not quite reach the bulk densities of 1.24 and 0.78 e/Å^3, respectively. The observed value of 0.73 e/Å^3 for Al is 6% below bulk value, which is close to the experimental error (5%). The observed value of 1.08 e/Å^3 for titanium is 13% below the bulk density. This can be explained by oxidation of the titanium by oxygen atoms and residual water on the mGO surface. For the latter, this contribution is expected to be minimal, since the titanium is deposited in high vacuum (10^{-7} Torr). Any water not evaporated or incorporated into the titanium layer could in principle affect device performance. When the observed electron density of the titanium layer (1.08 e/Å^3) is used to calculate the expected electron density for the fourth fatty acid layer, the electron density drops to 0.43 e/Å^3, which is in perfect agreement with the experimental value of 0.42 e/Å^3 (see Supporting Information for details). The relatively broad tail on the mGO layer in the electron density profile for the LB film without metal Figure 4b) has a thickness of about 15 Å and a roughness of about 8−9 Å. This layer thickness is consistent with a monolayer of GO (7.3 Å) and an uneven distribution of adsorbed water with an average thickness of a double layer (7.4 Å).[46,55,56] The relatively high double- and multilayer coverage (13 and 10 area %, respectively) also contributes to this deviation from the ideal monolayer thickness, but mainly contributes to the increased roughness. The 10 area % of uncovered film will contribute to a lower apparent thickness. For films where the mGO layer was compressed to a higher surface pressure before transfer, the tail broadens even further (see Supporting Information), which can be explained by a higher ratio of multilayers *versus* monolayers. The observed electron density of the mGO layer in the film without metal (0.53 e/Å^3) is slightly higher than the calculated value (0.51 e/Å^3), which is likely to be due to a contribution from an adlayer of water. For the more wrinkled samples the overall conclusion is the same, but with a rougher interface between the mGO and the titanium layer.

The very similar oscillations observed in the raw X-ray reflectivity data (Figure 4a), the very sharp interfaces, the conservation of all three cadmium peaks, and the perfect agreement between the expected and the observed increase in electron density are all strong evidence that mGO forms a highly effective barrier toward metal deposition. These results are in sharp contrast to unprotected lipid films covered with metal top layers, where a similar X-ray reflectivity analysis clearly showed a complete structural breakdown of the first two LB layers and metal penetration into the first ∼5 nm of the organic film.[19]

The demonstrated use of large-area LB films of mGO as protection layer suggests a solution to many of the previous problems with molecular crossbar junctions. Compared with multilayer films of CVD graphene or RGO, these mGO films have the advantage of simple and very gentle deposition. The in-plane electrical insulating nature of GO is expected to be of less importance since the extremely thin layer (0.7 nm) is expected to function only as a tunneling barrier, which can merely be considered as an additional contact resistance with no temperature dependence. Although CVD and RGO monolayer films hold the potential to decrease the contact resistance further, fabrication and in particular deposition of these materials are still challenging or even incompatible with physisorbed thin films.

CONCLUSION

In summary, we have shown using AFM and X-ray reflectivity that LB films of mosaic monolayers of GO can be transferred to structurally fragile LB films and function as a monoatomic barrier toward metal penetration, thus preventing structural reorganization altogether. These findings suggest that the recent demonstrations of functional vertical monolayer devices using multilayer graphene and RGO as

blocking layers[36−38] can be pushed to the monolayer limit and that such monolayers of GO could replace RGO, CVD, and pristine graphene for application in vertical devices.

MATERIALS AND METHODS

Wafer Cleaning. The substrates used were silicon(100) wafers covered with a natural oxide layer, bought from Si-Mat. The wafers were cut into 10 by 20 mm pieces, cleaned by 1−2 min sonication in chloroform, methanol, and milli-Q water, and then placed for 15 min in a 1:1:5 mixture of H_2O_2, NH_4OH, and milli-Q heated to 70 °C. The hydroxylated wafers were rinsed thoroughly with milli-Q water and stored in a beaker filled with milli-Q water until used.

Graphene Oxide Synthesis. A GO solution was prepared as described by Cote *et al.*[43] through the modified Hummers method using 0.5 g of graphite powder (Alfa Aesar, natural, 98% metal basis, −325 mesh, 41.6 mmol), 0.5 g of $NaNO_3$ (5.88 mmol), and 23 mL of H_2SO_4 (0.43 mol), which were stirred together on an ice-bath. A 3 g amount of $KMnO_4$ (19.0 mmol) was then slowly added as a powder. The solution was transferred to a 35 °C water bath and stirred for 1 h. A thick paste was formed. Then 40 mL of water was slowly added while stirring was continued and the temperature raised to 90 °C. A 100 mL portion of water was added followed by slow addition of 3 mL of H_2O_2 (97.9 mmol). The color turned from dark brown to yellow due to reduction of the residual permanganate and manganese dioxide (MnO_4, MnO_2) into manganese(II) by hydrogen peroxide. While still warm, the solution was filtered and washed with 100 mL of water. After washing, the filter cake could be dispersed in milli-Q water by shaking.

The GO was refined into mGO. A 12 mL amount of GO stock solution was subjected to five 2 min centrifugation steps at 1000 rpm to remove large aggregates. Small debris from the oxidation step was then removed by two high-speed centrifugation steps for 15 min at 8000 rpm. After each step the sediment was redissolved in 1:5 vol % milli-Q water/MeOH. For full exfoliation into monolayered GO, we found that 30 min was the optimal time for a tabletop sonication bath with a power output of 55.6 W/L. Small variations have been observed for identically prepared solutions prepared in parallel. The as-prepared mGO solution was then subjected to one last high-speed centrifugation step for 20 min at 8000 rpm to remove any debris created by the ultrasound. After this, the centrifugate was redispersed in 1:5 vol % mili-Q water/MeOH, which functioned as the spreading solvent for the LB deposition. Before deposition, the mGO solution was subjected to a 15 min 2500 rpm centrifugation step to remove any aggregates formed from the solvent change.

LB Assembly of Hybrid Films. LB films of cadmium(II) behenate were prepared from a 1 mg/mL chloroform solution of behenic acid. A 40 μL solution was carefully spread with a 100 μL Hamilton syringe onto a KSV minitrough with milli-Q water subphase containing 0.5 mM cadmium acetate and a pH in the range 6.3−7. The Langmuir film was allowed to equilibrate for 10 min before compression at 3 mm/min until a surface pressure of 30 mN/m was reached. The cadmium(II) behenate Langmuir film was then deposited by vertical LB transfer, starting with the substrate in the subphase. A transfer speed of 1 mm/min was applied for the first layer, while 3 mm/mm was used for the remaining layers. A surface pressure of 30 mN/m was maintained during transfer. After transferring four layers the sample was left in the subfase while the water surface was cleaned by carefully sucking up the fatty acids and replacing the removed subphase solution. mGO was carefully spread onto the water surface of a LB minitrough with a 100 μL Hamilton syringe. The drops should be as small as possible and placed alternately at each end of the trough. A 1−1.5 mL amount of mGO solution was deposited onto the surface. The mGO solution was deposited with a 1:5 volume ratio of milli-Q/MeOH spreading solution. The LB film could be compressed immediately after deposition. Compression was performed at 10 mm/min. Immediately after compression the film was transferred to the fatty acid−metal salt film by raising the sample vertically through the mGO film with a transfer speed of 1 mm/min. The typical transfer pressure was 15 mN/m for hybrid films and 25−30 mN/m for pure mGO LB films.

Vapor Deposition of Metals. The metals were evaporated in a custom-built chamber with the vacuum chamber kept at a pressure of 10^{-7} Torr. Titanium was deposited using an electron beam evaporator at a rate of 0.5−0.7 Å/s. Aluminum was deposited using thermal evaporation with a deposition rate of 0.8−1.0 Å/s.

Characterization. LB films were characterized with scanning electron microscopy (SEM; Hitachi S-4800), with low acceleration voltage (≈ 1 kV) and high current (15−20 μA), and AFM (Veeco Nanoscope V, PicoForce: Force spectroscopy control module) in tapping mode. X-ray reflectivity was performed at the synchrotron radiation facility at HASYLAB, Hamburg, Germany. High-quality specular reflectivity scans were performed at the BW2 beamline. The beam size was 1 mm × 0.1 mm, and the scans typically lasted 30−45 min. To reduce beam damage, the samples were moved twice to a new position during the measurement. The samples were then placed in a helium-filled Kapton-sealed chamber. The X-ray photon energy was 10.0 keV.

Conflict of Interest: The authors declare no competing financial interest.

Supporting Information Available: Stability of five-layered fatty acid−metal salt films and unprotected one- and four-layer films; detailed AFM and XRR data analysis. This material is available free of charge *via* the Internet at http://pubs.acs.org.

Acknowledgment. The authors acknowledge the financial support from the Danish-Chinese Center for Molecular Nanoelectronics funded by the Danish National Research Foundation, the Sino-Danish Center for Research and Education, the Danish Agency for Science, Technology and Innovation (10-082711), the National Natural Science Foundation of China (60911130231), and DANSCATT funded be the Natural Research Council. We also thank the staff of HASYLAB for their help and assistance.

REFERENCES AND NOTES

1. Aviram, A.; Ratner, M. A. Molecular Rectifiers. *Chem. Phys. Lett.* **1974**, *29*, 277–283.
2. Song, H.; Kim, Y.; Jang, Y. H.; Jeong, H.; Reed, M. A.; Lee, T. Observation of Molecular Orbital Gating. *Nature* **2009**, *462*, 1039–1043.
3. Lortscher, E.; Ciszek, J. W.; Tour, J.; Riel, H. Reversible and Controllable Switching of a Single-Molecule Junction. *Small* **2006**, *2*, 973–977.
4. Joachim, C.; Gimzewski, J. K.; Aviram, A. Electronics Using Hybrid-Molecular and Mono-Molecular Devices. *Nature* **2000**, *408*, 541–548.
5. Tao, N. J. Electron Transport in Molecular Junctions. *Nat. Nanotechnol.* **2006**, *1*, 173–181.
6. Akkerman, H. B.; Blom, P. W. M.; de Leeuw, D. M.; de Boer, B. Towards Molecular Electronics with Large-Area Molecular Junctions. *Nature* **2006**, *441*, 69–72.
7. Diez-Perez, I.; Hihath, J.; Lee, Y.; Yu, L. P.; Adamska, L.; Kozhushner, M. A.; Oleynik, I. I.; Tao, N. J. Rectification and Stability of a Single Molecular Diode with Controlled Orientation. *Nat. Chem.* **2009**, *1*, 635–641.
8. Akkerman, H. B.; de Boer, B. Electrical Conduction through Single Molecules and Self-Assembled Monolayers. *J. Phys.: Condens. Matter* **2008**, *20*, 013001.
9. Moth-Poulsen, K.; Bjornholm, T. Molecular Electronics with Single Molecules in Solid-State Devices. *Nat. Nanotechnol.* **2009**, *4*, 551–556.
10. Smit, R. H. M.; Noat, Y.; Untiedt, C.; Lang, N. D.; van Hemert, M. C.; van Ruitenbeek, J. M. Measurement of the Conductance of a Hydrogen Molecule. *Nature* **2002**, *419*, 906–909.

11. Moreland, J.; Ekin, J. W. Electron-Tunneling Experiments Using Nb-Sn Break Junctions. *J. Appl. Phys.* **1985**, *58*, 3888–3895.
12. Muller, C. J.; Ruitenbeek, J. M. v.; Jongh, L. J. d. Experimental Observation of the Transition from Weak Link to Tunnel Junction. *Phys. C* **1992**, *191*, 485–504.
13. Chen, Y.; Jung, G. Y.; Ohlberg, D. A. A.; Li, X. M.; Stewart, D. R.; Jeppesen, J. O.; Nielsen, K. A.; Stoddart, J. F.; Williams, R. S. Nanoscale Molecular-Switch Crossbar Circuits. *Nanotechnology* **2003**, *14*, 462–468.
14. Collier, C. P.; Wong, E. W.; Belohradsky, M.; Raymo, F. M.; Stoddart, J. F.; Kuekes, P. J.; Williams, R. S.; Heath, J. R. Electronically Configurable Molecular-Based Logic Gates. *Science* **1999**, *285*, 391–394.
15. Collier, C. P.; Mattersteig, G.; Wong, E. W.; Luo, Y.; Beverly, K.; Sampaio, J.; Raymo, F. M.; Stoddart, J. F.; Heath, J. R. A [2]Catenane-Based Solid State Electronically Reconfigurable Switch. *Science* **2000**, *289*, 1172–1175.
16. Heath, J. R.; Kuekes, P. J.; Snider, G. S.; Williams, R. S. A Defect-Tolerant Computer Architecture: Opportunities for Nanotechnology. *Science* **1998**, *280*, 1716–1721.
17. de Boer, B.; Frank, M. M.; Chabal, Y. J.; Jiang, W. R.; Garfunkel, E.; Bao, Z. Metallic Contact Formation for Molecular Electronics: Interactions between Vapor-Deposited Metals and Self-Assembled Monolayers of Conjugated Mono- and Dithiols. *Langmuir* **2004**, *20*, 1539–1542.
18. Haick, H.; Ghabboun, J.; Cahen, D. Pd *versus* Au as Evaporated Metal Contacts to Molecules. *Appl. Phys. Lett.* **2005**, *86*, 042113.
19. Hansen, C. R.; Sorensen, T. J.; Glyvradal, M.; Larsen, J.; Eisenhardt, S. H.; Bjornholm, T.; Nielsen, M. M.; Feidenhans'l, R.; Laursen, B. W. Structure of the Buried Metal-Molecule Interface in Organic Thin Film Devices. *Nano Lett.* **2009**, *9*, 1052–1057.
20. Loo, Y. L.; Willett, R. L.; Baldwin, K. W.; Rogers, J. A. Additive, Nanoscale Patterning of Metal Films with a Stamp and a Surface Chemistry Mediated Transfer Process: Applications in Plastic Electronics. *Appl. Phys. Lett.* **2002**, *81*, 562–564.
21. Loo, Y. L.; Lang, D. V.; Rogers, J. A.; Hsu, J. W. P. Electrical Contacts to Molecular Layers by Nanotransfer Printing. *Nano Lett.* **2003**, *3*, 913–917.
22. Zhou, C.; Deshpande, M. R.; Reed, M. A.; Jones, L.; Tour, J. M. Nanoscale Metal Self-Assembled Monolayer Metal Heterostructures. *Appl. Phys. Lett.* **1997**, *71*, 611–613.
23. Kushmerick, J. G.; Holt, D. B.; Yang, J. C.; Naciri, J.; Moore, M. H.; Shashidhar, R. Metal-Molecule Contacts and Charge Transport across Monomolecular Layers: Measurement and Theory. *Phys. Rev. Lett.* **2002**, *89*, 086802.
24. Slowinski, K.; Chamberlain, R. V.; Miller, C. J.; Majda, M. Through-Bond and Chain-to-Chain Coupling. Two Pathways in Electron Tunneling through Liquid Alkanethiol Monolayers on Mercury Electrodes. *J. Am. Chem. Soc.* **1997**, *119*, 11910–11919.
25. Novoselov, K. S.; Geim, A. K.; Morozov, S. V.; Jiang, D.; Zhang, Y.; Dubonos, S. V.; Grigorieva, I. V.; Firsov, A. A. Electric Field Effect in Atomically Thin Carbon Films. *Science* **2004**, *306*, 666–669.
26. Novoselov, K. S.; Geim, A. K.; Morozov, S. V.; Jiang, D.; Katsnelson, M. I.; Grigorieva, I. V.; Dubonos, S. V.; Firsov, A. A. Two-Dimensional Gas of Massless Dirac Fermions in Graphene. *Nature* **2005**, *438*, 197–200.
27. Zhang, Y. B.; Tan, Y. W.; Stormer, H. L.; Kim, P. Experimental Observation of the Quantum Hall Effect and Berry's Phase in Graphene. *Nature* **2005**, *438*, 201–204.
28. Wallace, P. R. The Band Theory of Graphite. *Phys. Rev.* **1947**, *71*, 622–634.
29. Bunch, J. S.; Verbridge, S. S.; Alden, J. S.; van der Zande, A. M.; Parpia, J. M.; Craighead, H. G.; McEuen, P. L. Impermeable Atomic Membranes from Graphene Sheets. *Nano Lett.* **2008**, *8*, 2458–2462.
30. Lee, C.; Wei, X. D.; Kysar, J. W.; Hone, J. Measurement of the Elastic Properties and Intrinsic Strength of Monolayer Graphene. *Science* **2008**, *321*, 385–388.
31. Reed, J. P.; Uchoa, B.; Joe, Y. I.; Gan, Y.; Casa, D.; Fradkin, E.; Abbamonte, P. The Effective Fine-Structure Constant of Freestanding Graphene Measured in Graphite. *Science* **2010**, *330*, 805–808.
32. Bae, S.; Kim, H.; Lee, Y.; Xu, X. F.; Park, J. S.; Zheng, Y.; Balakrishnan, J.; Lei, T.; Kim, H. R.; Song, Y. I.; *et al.* Roll-to-Roll Production of 30-Inch Graphene Films for Transparent Electrodes. *Nat. Nanotechnol.* **2010**, *5*, 574–578.
33. Yin, Z. Y.; Sun, S. Y.; Salim, T.; Wu, S. X.; Huang, X. A.; He, Q. Y.; Lam, Y. M.; Zhang, H. Organic Photovoltaic Devices Using Highly Flexible Reduced Graphene Oxide Films as Transparent Electrodes. *ACS Nano* **2010**, *4*, 5263–5268.
34. Pang, S. P.; Tsao, H. N.; Feng, X. L.; Mullen, K. Patterned Graphene Electrodes from Solution-Processed Graphite Oxide Films for Organic Field-Effect Transistors. *Adv. Mater.* **2009**, *21*, 3488–3491.
35. Zhao, J. P.; Pei, S. F.; Ren, W. C.; Gao, L. B.; Cheng, H. M. Efficient Preparation of Large-Area Graphene Oxide Sheets for Transparent Conductive Films. *ACS Nano* **2010**, *4*, 5245–5252.
36. Wang, G.; Kim, Y.; Choe, M.; Kim, T. W.; Lee, T. A New Approach for Molecular Electronic Junctions with a Multilayer Graphene Electrode. *Adv. Mater.* **2011**, *23*, 755–760.
37. Seo, S.; Min, M.; Lee, J.; Lee, T.; Choi, S.-Y.; Lee, H. Solution-Processed Reduced Graphene Oxide Films as Electronic Contacts for Molecular Monolayer Junctions. *Angew. Chem., Int. Ed.* **2012**, *51*, 108–112.
38. Li, T.; Hauptmann, J. R.; Wei, Z.; Petersen, S.; Bovet, N.; Vosch, T.; Hu, W.; Liu, Y.; Nygård, J.; Bjørnholm, T.; *et al.* Solution-Processed Ultrathin Chemically Derived Graphene Films as Soft Top Contacts for Solid-State Molecular Electronic Junctions. *Adv. Mater.* **2012**, *24*, 1333–1339.
39. Choi, S. H.; Risko, C.; Delgado, M. C. R.; Kim, B.; Bredas, J. L.; Frisbie, C. D. Transition from Tunneling to Hopping Transport in Long, Conjugated Oligo-Imine Wires Connected to Metals. *J. Am. Chem. Soc.* **2010**, *132*, 4358–4368.
40. Nitzan, A. Electron Transmission through Molecules and Molecular Interfaces. *Annu. Rev. Phys. Chem.* **2001**, *52*, 681–750.
41. Zasadzinski, J. A.; Viswanathan, R.; Madsen, L.; Garnaes, J.; Schwartz, D. K. Langmuir-Blodgett-Films. *Science* **1994**, *263*, 1726–1733.
42. Als-Nielsen, J.; McMorrow, D. *Elements of Modern X-Ray Physics*, 2nd ed.; Wiley: Hoboken, 2011.
43. Cote, L. J.; Kim, F.; Huang, J. X. Langmuir-Blodgett Assembly of Graphite Oxide Single Layers. *J. Am. Chem. Soc.* **2009**, *131*, 1043–1049.
44. Hummers, W. S.; Offeman, R. E. Preparation of Graphitic Oxide. *J. Am. Chem. Soc.* **1958**, *80*, 1339–1339.
45. Schwartz, D. K. Langmuir-Blodgett Film Structure. *Surf. Sci. Rep.* **1997**, *27*, 245–334.
46. Xu, K.; Cao, P. G.; Heath, J. R. Graphene Visualizes the First Water Adlayers on Mica at Ambient Conditions. *Science* **2010**, *329*, 1188–1191.
47. Stankovich, S.; Dikin, D. A.; Piner, R. D.; Kohlhaas, K. A.; Kleinhammes, A.; Jia, Y.; Wu, Y.; Nguyen, S. T.; Ruoff, R. S. Synthesis of Graphene-Based Nanosheets *via* Chemical Reduction of Exfoliated Graphite Oxide. *Carbon* **2007**, *45*, 1558–1565.
48. Luk, S. Y.; Wright, A. C.; Williams, J. O. On the Presence of Holes in Stearic-Acid Langmuir-Blodgett-Films Studied by Dark Field Electron-Microscopy. *Thin Solid Films* **1990**, *186*, 147–154.
49. Schwartz, D. K.; Viswanathan, R.; Garnaes, J.; Zasadzinski, J. A. Influence of Cations, Alkane Chain-Length, and Substrate on Molecular Order of Langmuir-Blodgett-Films. *J. Am. Chem. Soc.* **1993**, *115*, 7374–7380.
50. Konovalov, O. V.; Feigin, L. A. X-Ray Reflectivity Study of the Structure of Cadmium Stearate and Cadmium Behenate Langmuir-Blodgett-Films with a Small Amount of Layers. *J. Phys. IV* **1993**, *3*, 185–188.
51. Wang, H. Y.; Gao, S.; Huo, L. H.; Zhao, J. G. The One-Dimensional Polymer Poly[[aqua(2,2′-bipyridine)cadmium(II)]-μ-trans-stilbene-4,4′-dicarboxylato]. *Acta Crystallogr., Sect. E: Struct. Rep. Online* **2008**, *64*, M162–U1542.
52. Sposato, L. K.; LaDuca, R. L. Poly[1,4-Bis(4-pyridylmethyl)-piperazinediium [[Tetraaquacobaltate(II)]-μ-pyromellita-to-κ^2O(1):O(4)]dihydrate]. *Acta Crystallogr., Sect. E: Struct. Rep. Online* **2009**, *65*, M1709–U1779.

53. Martin, D. P.; Supkowski, R. M.; LaDuca, R. L. Cadmium Dicarboxylate Coordination Polymers Incorporating a Long-Spanning Organodiimine: *In Situ* Alkene Isomerization and an Unprecedented Chiral 6(5)8 Two-Dimensional Network. *Dalton Trans.* **2009**, 514–520.
54. Cote, L. J.; Kim, J.; Zhang, Z.; Sun, C.; Huang, J. X. Tunable Assembly of Graphene Oxide Surfactant Sheets: Wrinkles, Overlaps and Impacts on Thin Film Properties. *Soft Matter* **2010**, *6*, 6096–6101.
55. Jeong, H. K.; Lee, Y. P.; Lahaye, R. J. W. E.; Park, M. H.; An, K. H.; Kim, I. J.; Yang, C. W.; Park, C. Y.; Ruoff, R. S.; Lee, Y. H. Evidence of Graphitic AB Stacking Order of Graphite Oxides. *J. Am. Chem. Soc.* **2008**, *130*, 1362–1366.
56. Verdaguer, A.; Sacha, G. M.; Bluhm, H.; Salmeron, M. Molecular Structure of Water at Interfaces: Wetting at the Nanometer Scale. *Chem. Rev. (Washington, DC, U. S.)* **2006**, *106*, 1478–1510.